RPE **Radiation Physics & Engineering**
A Peer-Reviewed Journal
Published by K.N. Toosi University of Technology
http://rpe.kntu.ac.ir
Research Article

Radiation Physics and Engineering 2026; ?(?):?–?

Low energy proton beam characterization via a Slit-Scanner

Tayebeh Rahmanabadi[a], Hamid Jafari[a,*], Masoomeh Yarmohammadi Satri[b], Shahin Sanaye Hajari[b]

[a] *Department of Radiation Application, Faculty of Nuclear Engineering, Shahid Beheshti University, P.O. Box 19839-69411, Tehran, Iran*
[b] *Physic and Accelerators Research School, Nuclear Science and Technology Research Institute, P.O. Box 14395-836, Tehran, Iran*

HIGHLIGHTS

- Integrated beam diagnostic system designed for low-energy proton beams from ECR ion source.
- Faraday cup optimized using MCNPX simulations and COMSOL thermal analysis.
- Aluminum collector with 60° cone angle provides balance of performance and manufacturability.
- Helical cooling channel effectively removes heat from the conical collector region.
- Both SEM grid and slit scanner techniques yield Gaussian profiles with $R^2 > 0.99$.

ABSTRACT

Accurate measurement of beam current and transverse profile is critical for the development and optimization of low-energy ion beam systems. In this study, a comprehensive beam diagnostic setup integrating a Faraday cup, a slit-Scanner, and a secondary electron monitor (SEM) grid was designed and evaluated via MCNP simulations. Parametric studies were conducted to assess the influence of collector material and cone angle on Faraday cup performance, complemented by thermal analyses under realistic beam irradiation conditions. Simulation results indicated that variations in material and cone angle produced only marginal differences in collected current, suggesting comparable charge collection efficiency across configurations. Accordingly, the final design was guided by a multi-criteria framework encompassing electrical performance, thermal response, manufacturability, mechanical stability, weight, and cost. An aluminum collector with a 60 cone angle was selected as optimal, offering a balanced trade-off between performance and engineering practicality. Thermal simulations revealed peak temperatures in the conical region, underscoring the need for integrated cooling. Beam profile reconstruction using both the SEM grid and the slit-scanner yielded Gaussian distributions with full width at half maximum (FWHM) values of 76.7 mm and 68.7 mm, respectively. The narrower profile obtained from the slit-scanner reflects its superior spatial resolution, while the overall consistency between the two techniques confirms robust beam characterization. These findings validate the proposed diagnostic system as a reliable tool for current and profile measurements, providing a practical design framework applicable to low-energy ECR ion sources and accelerator facilities.

KEYWORDS
Ion beam diagnostic
Faraday cup
Slit-Scanner
Secondary electron monitor grid
MCNP simulation
Low-energy accelerator
ECR ion source

HISTORY
Received:
Revised:
Accepted:
Published:

1 Introduction

Particle accelerators and ion sources are fundamental tools in diverse fields, including nuclear physics, materials science, medical applications, and plasma research (Humphries, 2013). The performance and reliability of these systems are critically dependent on the quality, stability, and transport characteristics of the charged particle beams they produce (Reiser, 2008). Consequently, beam diagnostic systems are indispensable for monitoring beam behavior, optimizing transport efficiency, and ensuring overall accelerator performance (Minty and Zimmermann, 2003).

Among the various types of ion sources, Electron Cyclotron Resonance (ECR) ion sources have gained particular prominence due to their ability to deliver stable, high-current-density beams with low emittance. These advantageous features have led to their widespread adoption in accelerator facilities and experimental beamlines (Geller, 2018). For such sources, precise characterization

*Corresponding author: h_jafari@sbu.ac.ir

https://doi.org/

of the extracted beam is essential for evaluating extraction conditions and transport properties. This characterization typically involves measuring key beam parameters, including current, spatial distribution, profile, and divergence (Sortais, 2000). Faraday cups remain one of the most common and reliable devices for absolute beam current measurement, valued for their simple construction, high sensitivity, and robust charge collection capability (?). Recent developments have extended the role of Faraday cups beyond simple current monitoring; they now often serve as integral components of more complex diagnostic systems that, when combined with complementary techniques, enable comprehensive beam profile reconstruction. Their application scope has accordingly broadened from traditional accelerator diagnostics to medical accelerators, mass spectrometry, fusion experiments, and industrial irradiation systems, reflecting their versatility and ongoing technological evolution (Rawat et al., 2025).

For transverse beam profile characterization, slit-Faraday cup and secondary electron monitor (SEM) grid-Faraday cup configurations are frequently employed (?). The slit-Faraday cup technique offers high spatial resolution by sampling the beam intensity locally, making it particularly suitable for accurate profile measurements and beam optics optimization in low-energy transport lines (You et al., 2015a). In contrast, SEM grids infer the beam profile by detecting secondary electrons emitted from thin metallic wires, enabling fast, near-real-time monitoring with satisfactory spatial resolution-an attractive feature for routine operation in modern accelerators (Baxter et al., 2025).

In this work, a diagnostic system is developed to characterize the proton beam extracted from an ECR ion source. The study includes the design and optimization of a Faraday cup collector, where material selection, geometry, and thermal behavior are evaluated using MCNP particle transport simulations and COMSOL thermal analysis. In addition, the transverse beam profile is reconstructed through slit-Faraday cup and SEM grid-Faraday cup configurations, and Gaussian fitting is applied to quantify the beam spreading and spatial distribution.

The main contribution of this study is the integrated optimization of a diagnostic setup specifically tailored for lowenergy proton beams. While the individual diagnostic techniques are well established, their combined use together with a systematic optimization of the collector has not been fully addressed for this application. The proposed design provides a practical balance between electrical performance, thermal stability, and engineering constraints, and offers complementary current and profile measurement capabilities. The structure of the paper is as follows: Section 2 presents the Faraday cup design and optimization; Section 3 describes the profilemeasurement methods; Section 4 discusses the simulation and experimental results; and Section 5 summarizes the main findings.

2 Design and optimization of the Faraday Cup

Accurate beam current measurement with a Faraday cup depends not only on its electrical characteristics but also on a complex interplay of geometrical configuration, construction material, thermal behavior, and mechanical integrity. These factors collectively govern charge collection efficiency, measurement stability, and long-term operational reliability. Consequently, the development of a high-performance Faraday cup necessitates a comprehensive optimization framework that simultaneously accounts for particle transport, secondary electron suppression, heat dissipation, and fabrication constraints (Rawat et al., 2025). A primary source of measurement uncertainty in Faraday cups is the emission of secondary electrons when incident ions strike the collector surface. These low-energy electrons, if allowed to escape, reduce the net collected charge and introduce systematic errors in the measured current. To mitigate this effect, a negatively biased suppressor electrode is typically placed at the entrance aperture. The resulting electrostatic field redirects secondary electrons back into the collector cavity, thereby enhancing charge collection efficiency and measurement accuracy (Ehwald et al., 2023). The effectiveness of this suppression mechanism, however, is highly sensitive to the applied bias voltage. An insufficient suppressor voltage generates a weak electrostatic field near the entrance, failing to retain all emitted electrons and allowing a fraction to escape-thus degrading the measurement fidelity (Harasimowicz and Welsch, 2010).

Beyond secondary electron suppression, the collector geometry plays a decisive role in the internal physical processes of the detector. The geometrical configuration influences the transport of backscattered particles, the recapture probability of secondary electrons, the internal electrostatic field distribution, and the spatial pattern of beam-induced heat deposition. Compared with conventional cylindrical collectors, conical geometries offer distinct advantages: they provide a larger effective interaction surface, promoting a more uniform distribution of deposited thermal power and mitigating localized hot spots. Moreover, secondary electrons and backscattered ions generated within a conical cavity undergo multiple interactions with the inclined inner walls before reaching the entrance aperture, significantly increasing their recapture probability and reducing particle escape (Brown, 2004). In addition, the conical shape fosters a more favorable electrostatic potential distribution inside the collector, resulting in stronger confinement of low-energy secondary electrons and improved measurement accuracy and operational stability (?). These attributes collectively establish the collector geometry as one of the most influential parameters in Faraday cup optimization.

Based on these considerations, an integrated, simulation-driven design methodology was adopted in the present work to optimize the detector prior to fabrication. The optimization process proceeded through three sequential stages. First, Monte Carlo particle transport simulations (using MCNP) were performed to investigate the effects of collector geometry and construction material on charge collection performance. Second, thermal analyses (using COMSOL) were conducted to evaluate the temperature distribution under proton beam irradiation and to identify regions susceptible to high thermal loading. Finally, the optimized configuration was translated into a three-dimensional mechanical model to verify its structural feasibility and manufacturability. The detailed methodology employed in each stage of the design and optimization process is presented in the following subsections.

2.1 MCNP Modeling and Geometrical Optimization

To optimize the Faraday cup design prior to fabrication, Monte Carlo simulations were conducted using MCNP version 2.6.0. Within this framework, a threedimensional model of the proposed collector, consisting of a conical section attached to a cylindrical body, was constructed to evaluate the effects of geometry and material on current-collection performance. A monoenergetic 45 keV proton beam, defined using the SDEF source card, was directed normally onto the collector entrance, and 1.0×10^6 particle histories were simulated to ensure statistically converged results. Proton transport and particle-matter interactions were modeled using the ENDF70PROT continuousenergy proton crosssection library, which is specifically designed for proton transport simulations in MCNP.

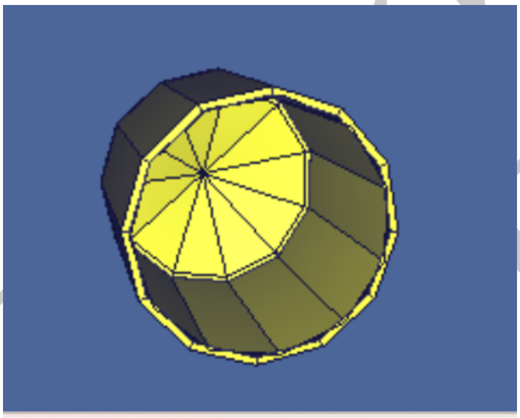

Figure 1: Three-dimensional MCNP view of the optimized Faraday cup with a conical collector, as implemented in the MCNP simulations for beam current evaluation.

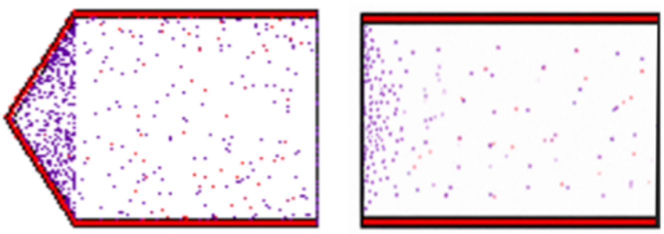

(a) (b)

Figure 2: MCNP-simulated proton trajectories in (a) conical and (b) cylindrical Faraday cup geometries under identical beam conditions.

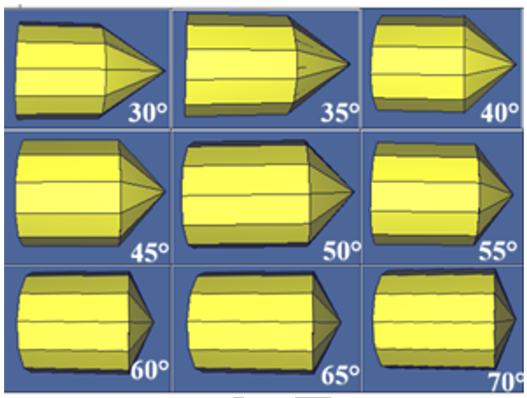

Figure 3: Three-dimensional MCNP models of conical Faraday cup geometries with different collector angles ranging from 30° to 70°, used to evaluate the effect of cone angle on beam current collection performance.

The collected beam current was computed using the F1 surface current tally, which records the net current crossing a specified surface. The statistical uncertainty associated with the F1 tally was determined to be 0.07%, indicating excellent numerical convergence and a high level of confidence in the simulation outcomes. The resulting data were then used to guide the selection of the collector geometry and material composition prior to fabrication, providing a robust and reliable foundation for the final design of the Faraday cup (Ehwald et al., 2023).

A qualitative comparison of particletransport behavior between cylindrical and conical collector geometries is shown in Fig. 2. Under identical beam conditions, the incident protons undergo multiple scattering interactions before thermalization. In the cylindrical collector, a significant fraction of scattered particles remains near the entrance, increasing the probability of backscattering or escape. In contrast, the converging walls of the conical collector redirect scattered particles deeper into the cavity, promoting successive wall collisions and reducing particle loss at the aperture. This improved confinement enhances chargecollection efficiency, consistent with the results presented earlier. Based on these observations, the conical geometry was selected as the reference configuration for subsequent optimization of the collector angle and material (Brown, 2004; **?**).

To evaluate the influence of collector angle on the collected beam current, MCNP simulations were performed for cone angles ranging from 30° to 70°, while all other beam and geometric parameters were kept constant. This parametric study enabled an isolated assessment of the angular effect on particle transport and charge collection. As shown in Fig. 3, varying the cone angle modifies the internal collision geometry and the likelihood of particle-wall interactions prior to full energy deposition. Smaller angles generally enhance confinement through more effective multiple reflections, but the optimal angle cannot be determined solely from collection performance. Practical manufacturability considerations, including machining complexity, tool accessibility, dimensional precision, overall manufacturing feasibility, and production cost, must also be taken into account. Sharper angles require deeper machining and reduced tool clearance, increasing the risk of dimensional inaccuracies and higher fabrication cost, whereas larger angles are easier to machine but provide weaker confinement. The quantitative results of this angular study are presented in Section 4, where a balanced tradeoff between performance and manufacturability is established.

Following the geometrical optimization, the influence of collector material on beamcurrent collection was examined using MCNP. Proton interactions with the collector surface depend on the atomic and physical properties of the material, which can affect charge deposition and the measured current. To evaluate this effect, four commonly used engineering materials in chargedparticle diagnostics-copper, aluminum, stainless steel, and brass-were selected as candidates. All simulations were performed using the optimized conical geometry under identical beam conditions, ensuring that any differences in collected current arose solely from material properties. This approach enabled an independent assessment of materialrelated effects before incorporating additional engineering considerations such as thermal conductivity, mechanical strength, and cost. A quantitative comparison of the simulated beam currents for each material is presented in Section 4, forming the basis for the final material selection.

2.2 Thermal Analysis Using COMSOL Multiphysics

While the MCNP simulations provided an optimized collector geometry with enhanced beam collection efficiency, thermal performance remains a critical design consideration for continuous operation of the Faraday cup. The kinetic energy deposited by the incident proton beam is converted into heat within the collector volume, giving rise to localized temperature increases that can adversely affect measurement stability, material integrity, and the long-term reliability of the diagnostic system (Ashcroft and Mermin, 1976). Consequently, a comprehensive thermal analysis is essential to verify that the optimized geometry meets operational requirements under realistic beam irradiation conditions.

Three-dimensional thermal simulations were performed using COMSOL Multiphysics to investigate heat generation and dissipation within the optimized Faraday cup. The simulations covered a range of proton beam energies from 45 to 55 keV and beam currents from 500 μA to 30 mA, reflecting the typical operating envelope of the ECR ion source. The effects of collector material, beam power, and geometrical configuration on the steady-state temperature distribution were systematically evaluated.

The thermal behavior of the collector is of particular importance because the electrical resistivity of metallic materials increases with temperature. Excessive heating can induce thermal drift in the measured current, introduce thermal stresses, and cause geometric deformation of the collector, all of which compromise measurement accuracy and reproducibility (Ashcroft and Mermin, 1976). In practical beam diagnostic systems, maintaining the collector temperature below approximately 80-100 °C is generally recommended to preserve both electrical stability and dimensional precision during prolonged operation (**?**).

To identify the most suitable collector material prior to the implementation of an active cooling system, the four candidate materials, copper, aluminum, stainless steel, and brass, were comparatively investigated under identical beam conditions. The thermal simulations considered the heat transfer mechanisms of conduction within the collector body and convection from the external surfaces, while radiation losses were assumed to be negligible due to the relatively moderate temperature levels expected in this study. The quantitative results of the thermal analysis, including maximum temperatures, temperature gradients, and thermal stress distributions, are presented and discussed in Section 4, providing the basis for the final material selection and cooling strategy.

2.2.1 Thermal Performance of Candidate Collector Materials

The thermal response of the Faraday cup under proton beam irradiation is strongly governed by the thermophysical properties of the collector material, particularly thermal conductivity and specific heat capacity. To evaluate this dependence, the four candidate materials-copper, aluminum, stainless steel, and brass-were subjected to identical beam conditions in the COMSOL simulations, and their transient thermal behavior was compared.

As presented in Fig. 4, the temperature evolution exhibits a characteristic rapid rise during the initial stage of beam irradiation, corresponding to the concentrated deposition of beam power within a relatively small interaction volume at the collector surface. Subsequently, as heat propagates through the collector body via conduction, the rate of temperature increase gradually diminishes, and the system approaches a quasisteadystate condition where the heat input is balanced by dissipation to the surroundings. The colored curves in this Figure represent the temperature response of each material under different beam powers, as indicated in the legend. The numerical values annotated directly on the curves denote the time at which the material reaches its melting point for that specific power level. As expected, no melting occurs at the lowest power, whereas both intermediate and maximum powers lead to melting, with the highest power producing the shortest melting time due to the more rapid thermal rise.

Among the investigated materials, copper demonstrates the most favorable thermal performance, exhibiting the lowest peak temperature and the shortest time to reach thermal equilibrium. This behavior is attributed to copper's exceptionally high thermal conductivity (approximately 401 $W.m^{-1}.K^{-1}$), which facilitates efficient heat spreading from the beam interaction zone throughout the entire collector volume. Conversely, stainless steel, with its relatively low thermal conductivity (approximately 16 $W.m^{-1}.K^{-1}$), shows the highest temperature rise, indicating less efficient heat distribution and greater localized heat accumulation. Aluminum and brass exhibit intermediate thermal responses, consistent with their respective thermal conductivities of approximately 237 $W.m^{-1}.K^{-1}$

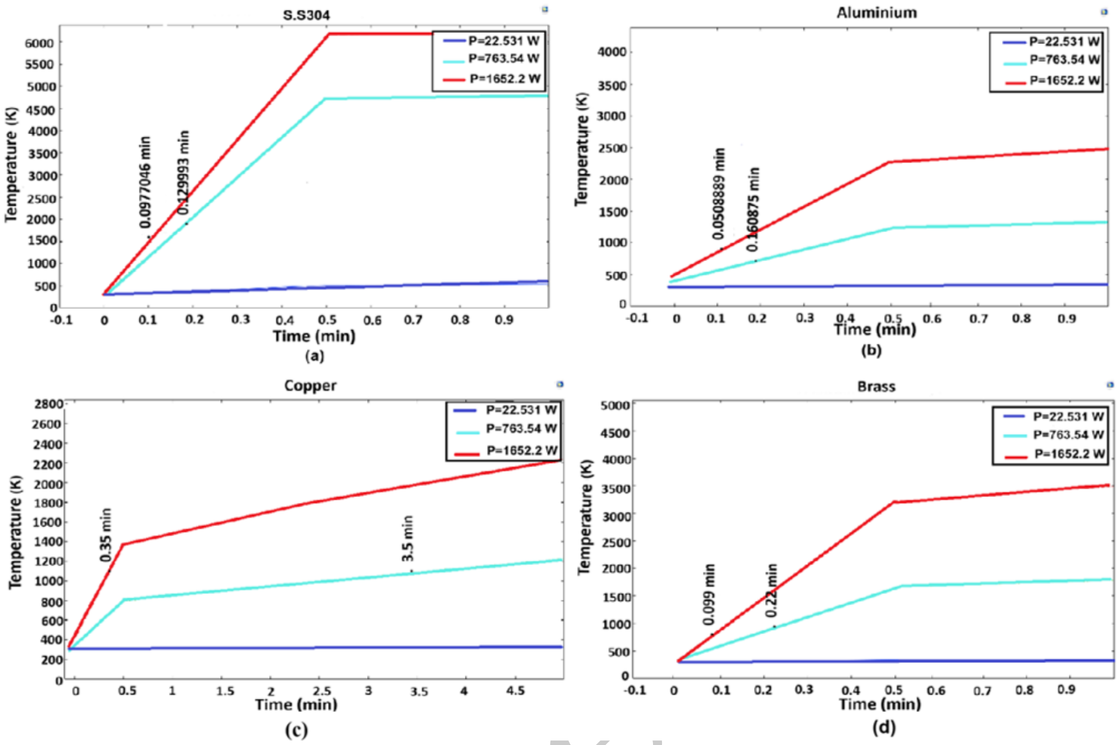

Figure 4: Temperature evolution over time for different collector materials (a) stainless steel, (b) aluminum, (c) Copper, and (d) brass simulated using COMSOL Multiphysics under identical beam irradiation conditions.

and 109 $W.m^{-1}.K^{-1}$.

These results demonstrate that thermal conductivity is the dominant factor governing heat dissipation and the steadystate temperature distribution inside the Faraday cup. Although the four candidate materials exhibit different thermal responses, all remain within acceptable temperature limits under the simulated operating conditions. This observation indicates that thermal behavior alone is insufficient for distinguishing between the candidate materials, and therefore the thermal analysis presented here should be regarded as one component of a broader multicriteria evaluation framework.

The final collector configuration will be determined by combining the thermalanalysis results with particletransport performance and practical engineering considerations such as manufacturability, mechanical stability, structural integrity, weight, and fabrication cost. This integrated approach ensures that the selected material and geometry achieve an optimal balance between scientific performance and engineering practicality.

2.2.2 Effect of Collector Angle on Thermal Performance

The influence of the collector cone angle on the transient thermal response of the four candidate materials is shown in Fig. 5. Under identical beamloading conditions, all materials exhibit an initial rapid temperature rise followed by a gradual approach to steady state. Although the overall heating trend is similar for all angles, the equilibrium temperature increases moderately as the cone angle is raised from 30° to 65°, reflecting changes in the heattransfer path and the spatial distribution of deposited power.

For each material, the temperature differences between the investigated angles remain relatively small, indicating that thermal behavior alone does not provide a strong basis for selecting the cone angle. Accordingly, the final configuration was determined through a multicriteria decisionmaking process that integrated MCNP particle-transport performance, thermal response, manufacturability, and mechanical design constraints. This approach ensured an appropriate balance between beamcollection efficiency, thermal stability, and engineering practicality.

2.2.3 Temperature Distribution and Localization of Thermal Load

The spatial temperature distribution for the investigated materials under the highest beampower condition is shown in Fig. 6. Despite differences in peak temperature arising from variations in thermal conductivity, all materials exhibit a similar pattern: the maximum temperature is concentrated near the conical tip, where most of the proton beam energy is deposited, and decreases gradually along the axial direction as heat is conducted through the collector body. This indicates that the thermal load is highly localized at the tip, where the highest thermal stresses are expected during continuous operation, potentially affecting mechanical integrity and longterm reliability.

Based on these findings, the cooling strategy was designed to focus on the conical section, where the thermal load is concentrated. Targeting this region maximizes heat removal while simplifying the mechanical layout and reducing overall system complexity. The performance of

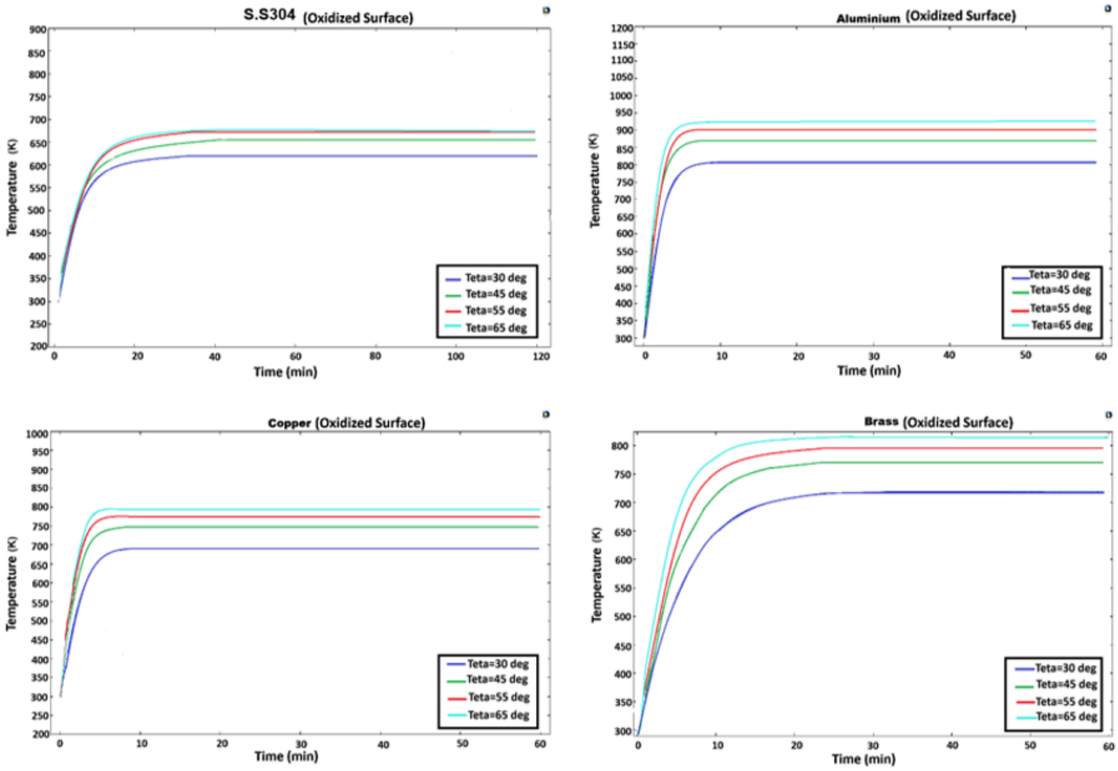

Figure 5: Effect of collector cone angle on the transient temperature evolution of different collector materials obtained from COMSOL thermal simulations.

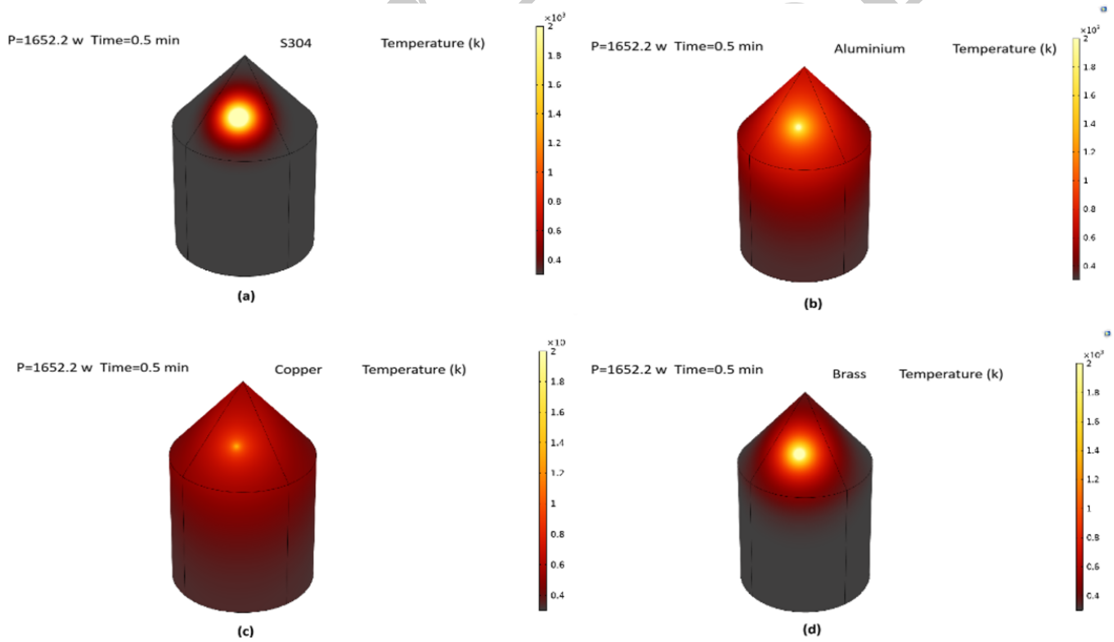

Figure 6: Temperature distribution in the Faraday cup collector obtained from COMSOL simulations under beam irradiation for different materials: (a), (b), (c) and (d).

this localized cooling approach is discussed in the following section.

2.2.4 Cooling System Design Based on Thermal Analysis

Based on the thermal analysis, an active watercooling system was implemented to maintain the collector temperature within a safe operating range under highpower beam conditions. The cooling channel consists of a fiveturn helical tube wrapped around the conical section, with a total length of approximately 85 cm and a pitch of about 2 cm. This spiral configuration was selected to maximize heat removal from the region of highest thermal load while preserving a compact and manufacturable design.

The thermal performance of the cooling system was

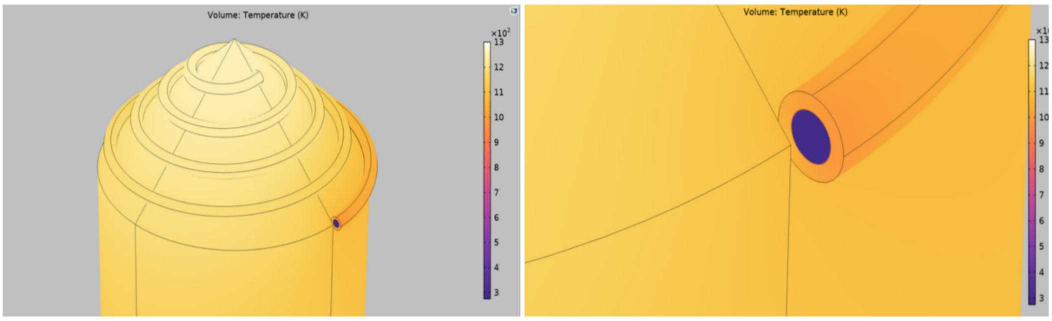

Figure 7: Temperature distribution of the cooled Faraday cup with the helical water-cooling channel under maximum beam power.

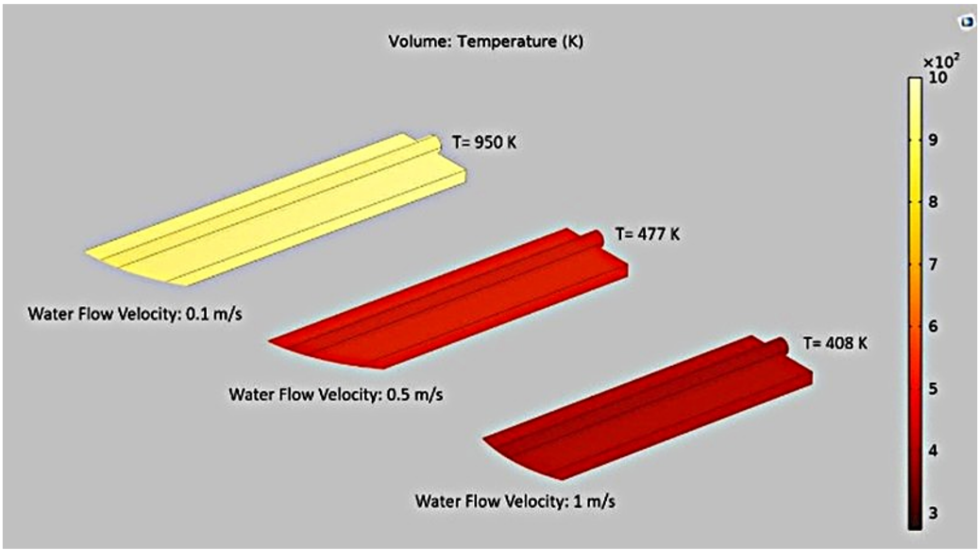

Figure 8: Thermal performance of the cooling channel as a function of water velocity under maximum beam power.

evaluated using COMSOL under maximum beampower conditions. As shown in Fig. 7, the cooling channel significantly reduces the peak temperature compared with the uncooled configuration, with the remaining hotspot confined to a small area near the beam impact point. The rest of the collector operates at substantially lower temperatures, confirming that localized cooling around the conical section provides effective thermal management without requiring fullbody cooling and thereby simplifies the mechanical design.

To optimize the cooling system, the effect of coolant flow velocity on thermal performance was examined under identical beamloading conditions. As shown in Fig. 8, increasing the water velocity from 0.1 to 0.5 m.s^{-1} significantly reduces the outlet temperature, reflecting enhanced convective heat transfer. Further increasing the velocity to 1.0 m.s^{-1} yields only a modest additional decrease, indicating that cooling performance approaches a plateau at higher flow rates. Beyond approximately 0.5 m.s^{-1}, thermal improvements become marginal while the required pumping power and mechanical stress on the cooling circuit increase.

The corresponding evolution of the maximum coolant temperature is presented in Fig. 9, which shows a consistent trend. At a flow velocity of 0.1 m.s^{-1}, the coolant temperature reaches approximately 95 °C, indicating insufficient heat removal due to limited convective heat transfer. Increasing the velocity to 0.5 m.s^{-1} results in a substantial temperature reduction, while a further increase to 1.0 m.s^{-1} provides a smaller additional improvement. These results confirm that the most significant enhancement in cooling performance is achieved by raising the flow velocity from 0.1 to 0.5 m.s^{-1}, whereas higher velocities yield diminishing returns.

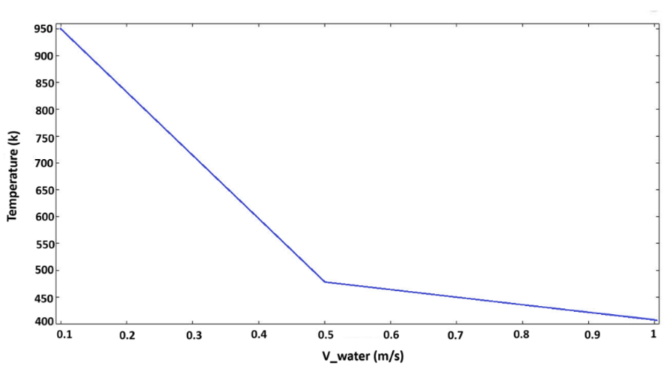

Figure 9: Effect of cooling-water velocity on the peak coolant temperature.

Table 1: Comparative assessment of physical, thermal, and engineering properties of candidate collector materials (Cu, Al, SS 304, and brass) for Faraday cup fabrication (?Valizadeh et al., 2014).

Property/Criteria	Copper (Cu)	Aluminum (Al)	Stainless Steel (SS)	Brass
Electrical conductivity	Excellent	Good	Poor	Moderate
Thermal conductivity	Excellent	Very Good	Poor	Moderate
Secondary electron emission yield (SEY)	Low	High	Moderate	High
Vacuum compatibility	Good	Good	Excellent	Moderate
Machinability	Difficult	Excellent	Difficult	Excellent
Relative Cost	High	Low	Moderate	Moderate
Mechanical stability	Moderate	Moderate	Excellent	Good

Based on these findings, a coolant velocity of 1.0 $m.s^{-1}$ would select for the final design. Although the improvement from 0.5 to 1.0 $m.s^{-1}$ is relatively modest, this velocity provides an additional safety margin to ensure reliable thermal stabilization of the Faraday cup under the maximum operating beam power, while remaining practically achievable with standard pumping systems.

2.3 Three-Dimensional Modeling of the Faraday Cup Using SolidWorks

Following the geometrical optimization through MCNP simulations and the thermal evaluation performed using COMSOL Multiphysics, the final mechanical model of the Faraday cup was developed using SolidWorks. The three-dimensional CAD model incorporates the optimized collector geometry with a cone angle of 60°, together with the final structural dimensions adopted for fabrication (Fig. 10). Section views were employed during the design process to verify the internal cavity geometry, ensure dimensional consistency, and identify any potential manufacturing conflicts prior to prototyping. The resulting model served as the basis for the fabrication of the experimental prototype, providing a precise digital representation of the detector for subsequent manufacturing and assembly.

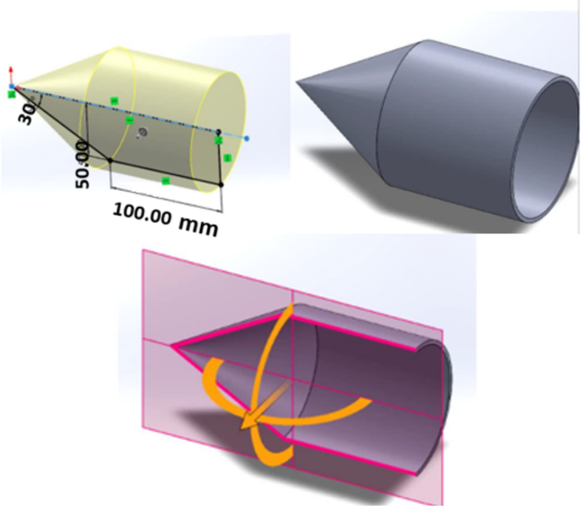

Figure 10: Three-dimensional CAD model of the conical Faraday cup developed in SolidWorks.

2.3.1 Multi-Criteria Material Selection

To complement the numerical simulations, the four candidate collector materials, copper, aluminum, stainless steel, and brass, were evaluated based on a comprehensive set of practical engineering criteria. These included electrical conductivity, thermal conductivity, secondary electron emission characteristics, vacuum compatibility, machinability, mechanical stability, and material cost. A qualitative comparison of the investigated materials is summarized in Table 1, which provides an overview of the relative performance of each candidate across the selected evaluation metrics.

The evaluation criteria were selected because they directly affect the electrical performance, thermal response, and practical manufacturability of the collector. Electrical and thermal conductivities determine chargecollection efficiency and heat dissipation, while vacuum compatibility prevents outgassing in ultrahighvacuum environments. Machinability and mechanical stability influence fabrication quality and longterm dimensional integrity, and cost represents a practical constraint for system development. The materialselection process integrated the MCNP particletransport results, COMSOL thermal analyses, and the engineering considerations summarized in Table 1. Although copper has higher electrical and thermal conductivity than aluminum, the MCNP simulations showed only marginal differences in collected current among the four materials, indicating that electrical conductivity alone does not strongly differentiate the candidates. In contrast, the thermal analyses revealed notable variations: stainless steel exhibited the highest temperature rise due to its low thermal conductivity, whereas aluminum showed moderate peak temperatures and efficient heat spreading.

Aluminum also provides several practical advantages. Its low density (≈ 2.7 $g.cm^{-3}$) results in a significantly lighter collector compared with copper or stainless steel, improving mechanical handling and mounting. Its excellent machinability enables precise fabrication of the conical geometry with reduced tool wear. Additionally, aluminum is vacuum compatible, readily available, and costeffective. Based on the combined simulation results and engineering considerations, aluminum was selected as the optimal collector material. This choice represents a balanced compromise between electrical performance, thermal behavior, mechanical stability, manufacturability, weight, and cost, ensuring that the final design satisfies both scientific and engineering requirements.

3 Beam Profile Measurements

Precise characterization of the transverse beam profile is essential for evaluating beam transport quality, optimizing beam optics, and ensuring the efficient performance of ion source diagnostic systems. Beam profile measurements provide critical information regarding beam focusing, spatial intensity distribution, and transverse beam behavior in low-energy accelerator beamlines. These parameters are fundamental for understanding beam extraction conditions, identifying transport inefficiencies, and optimizing the performance of the overall beamline system. In the present work, the transverse profile of the 45 keV proton beam extracted from the ECR ion source was characterized using two complementary diagnostic techniques: the slit-Faraday cup method and the SEM grid-Faraday cup system. These diagnostic approaches were employed to evaluate the spatial distribution of the extracted beam and compare their performance in beam profile measurements.

3.1 Slit-Faraday Cup Method

The slit-Faraday cup method is a most widely established interceptive techniques for transverse beam profile measurements due to its high spatial resolution and relatively simple diagnostic configuration (You et al., 2015b). In this method, a narrow slit is scanned transversely across the beam path, and the transmitted particles are collected by a Faraday cup positioned behind the slit. The resulting intensity as a function of slit position provides a direct measure of the beam's transverse spatial distribution. The selection of slit material is critical to the measurement accuracy and operational stability of the system (Sun, 2017). The slit material must exhibit low secondary electron emission yield to minimize measurement artifacts, adequate thermal resistance to withstand direct beam irradiation without deformation, and sufficient mechanical stability to maintain dimensional precision over extended use. Additionally, practical considerations-including fabrication feasibility, machining characteristics, and material cost-were taken into account during the design process. Based on these criteria, molybdenum was selected as the optimum slit material due to its high melting point (2623 °C), excellent thermal stability, low secondary electron emission yield, and suitable mechanical strength under beam irradiation conditions.

In the present work, the slit was scanned incrementally across the beam path, and at each position, the transmitted proton flux entering the Faraday cup was recorded. To quantify the intensity of particles transmitted through the slit aperture, the MCNP F2 tally was used to calculate the proton flux crossing the entrance surface of the Faraday cup positioned immediately behind the slit. This configuration enabled direct evaluation of the transmitted beam intensity as a function of slit displacement without redundancy in the tally definition. This approach provided a high-resolution spatial sampling of the beam intensity distribution, which was subsequently used to reconstruct the transverse beam profile through Gaussian fitting, as described in Section 4.

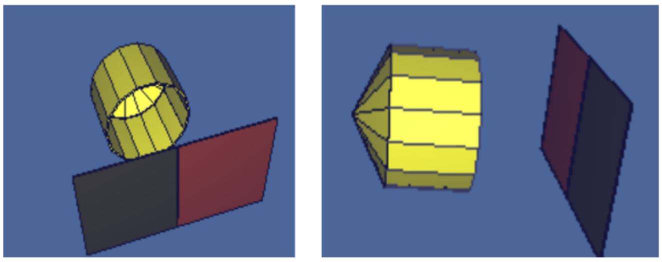

Figure 11: SolidWorks model of the slitFaraday cup diagnostic assembly used for transverse beam profile reconstruction.

3.2 SEM Grid and Faraday Cup Method

The operating principle of the SEM grid is based on the phenomenon of secondary electron emission, in which charged particles strike the surface of a thin metallic wire and secondary electrons are emitted with a yield that is proportional to the local beam intensity incident upon that wire. By measuring the current collected from each wire across the array, the transverse beam profile can be reconstructed with high temporal resolution (Baxter et al., 2025) .

In the present work, the SEM grid system was employed for transverse beam profile measurements of the extracted 45 keV proton beam (Barale et al., 1979). In this diagnostic arrangement, the movable SEM grid was positioned directly in the beam path, while the Faraday cup was located downstream the grid structure (Figs. 12 and 13). The SEM grid consisted of 48 tungsten wires distributed across the beam cross-section with non-uniform spacing. A denser wire arrangement was implemented near the central region of the grid in order to achieve higher spatial resolution in the beam core, where the particle intensity and profile gradients are most significant. Conversely, larger wire spacing was employed toward the outer regions of the beam, where the particle intensity is lower and the profile variations are smoother. This non-uniform design optimizes the trade-off between spatial resolution and measurement coverage, ensuring that the most critical region of the beam profile is sampled with maximum detail. It should be noted that the singleaxis SEM grid configuration used in this study represents a simplification appropriate for the simulation framework. In practical accelerator systems, SEM grids are typically installed in both horizontal and vertical orientations to provide full twodimensional transverse beam profiles.

The selection of tungsten as the wire material was based on several key material and operational considerations. Tungsten possesses a very high melting point (3422 °C), excellent thermal resistance, suitable mechanical rigidity, and high structural stability under charged particle irradiation conditions (Minty and Zimmermann, 2003). These characteristics make tungsten particularly well suitable for thin-wire diagnostic structures exposed to direct beam interaction. Furthermore, the high mechanical durability and low deformation probability of tungsten wires enhance the stability and reliability of beam profile measurements during prolonged operation, even under high beam current conditions.

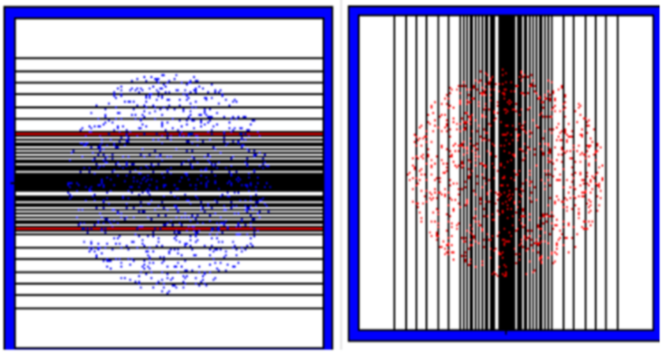

Figure 12: MCNP geometric model of the SEM grid assembly used for transverse beam profile measurements.

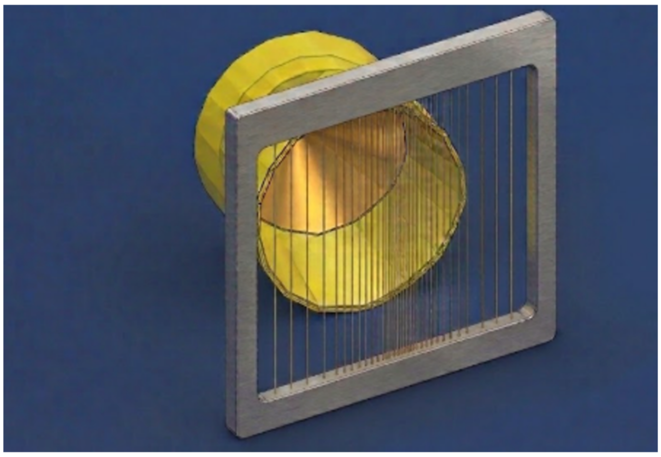

Figure 13: CAD model of the SEM gridFaraday cup diagnostic assembly used for beam profile measurements.

When the proton beam interacts with the tungsten wire array, The signals generated on the individual wires are recorded and processed to reconstruct the transverse beam intensity distribution. In the simulation framework, each tungsten wire was modeled as an independent volumetric cell to enable detailed analysis of particle interactions within the wire structure. The average particle flux within each wire was obtained using the MCNP F4 tally, which provides a volumeaveraged measure of proton intensity while accounting for scattering and local variations inside the wire. The resulting values were then used to reconstruct the transverse beam profile, yielding a simulated intensity distribution suitable for direct comparison with the slitscanner results and experimental measurements.

4 Results and Discussion

4.1 Beam Current Measurement Using the Faraday Cup

To evaluate the influence of collector material on the current collection performance of the Faraday cup, systematic MCNP simulations were performed for four candidate materials, copper, aluminum, stainless steel, and brass, while maintaining a fixed collector cone angle of 60°. The collected beam current was calculated for two distinct beam currents levels: 500 μA and 30 mA, representing low- and high-intensity operating conditions of the ECR ion source.

As presented in Fig. 14, copper exhibits the highest collected current, while aluminum results in the lowest measured value for both beam current levels. The observed differences are relatively small and can be attributed primarily to material, dependent variations in particle backscattering and energy deposition mechanisms. Although material-dependent effects are evident, the relatively small variation among the investigated materials suggests that the current collection process is predominantly governed by the collector geometry. Furthermore, the moderate beam energy of 45 keV limits the magnitude of material-dependent effects, resulting in comparable current collection performance for all investigated materials. The small differences indicate that, at the investigated beam energy, material-dependent effects remain secondary compared with geometrical factors.

Following the selection of aluminum as the collector material, the influence of the collector cone angle on the measured beam current was systematically investigated. Simulations were performed for cone angles ranging from 30° to 70° in 5° increments, at beam currents of 500 μA and 30 mA, while keeping all other parameters constant.

Figure 15 illustrates the variation of the collected current as a function of the collector cone angle. The results indicate that the collected current gradually decreases as the cone angle increases from 30° to 70°. Although the highest collected current appears at 30°, this value represents an overestimation caused by the strong confinement of scattered particles within the deep conical cavity at this angle. Because this artificially enhances the measured current, the 30° configuration cannot be considered a reliable operating angle and is therefore excluded from the optimization process. For angles above 30°, smaller cone angles still provide stronger particle confinement, increasing the probability of multiple wall interactions before escape. As the cone angle increases, the confinement capability is slightly reduced, leading to a modest decrease in collected current. Nevertheless, the overall trend remains relatively weak, indicating that efficient charge collection is maintained throughout the investigated angular range.

4.2 Beam Profile Measurement

To characterize the initial proton source used in the simulations, both the onedimensional transverse profile and the twodimensional spatial distribution were obtained using MCNPX mesh tallies. Figure 16 presents the extracted source profiles, which form the baseline input for the subsequent beamtransport analysis.

The proton source was characterized using MCNPX mesh tallies to obtain both its transverse and spatial intensity distributions. The onedimensional profile shows a smooth and symmetric distribution around the beam axis, and the Gaussian fit closely matches the MCNPX data, confirming that the source can be accurately represented by a Gaussian model for transport calculations. The extracted parameters ($\sigma = 31.00$ mm, FWHM $= 72.94$ mm) define the effective beam width at the source plane.

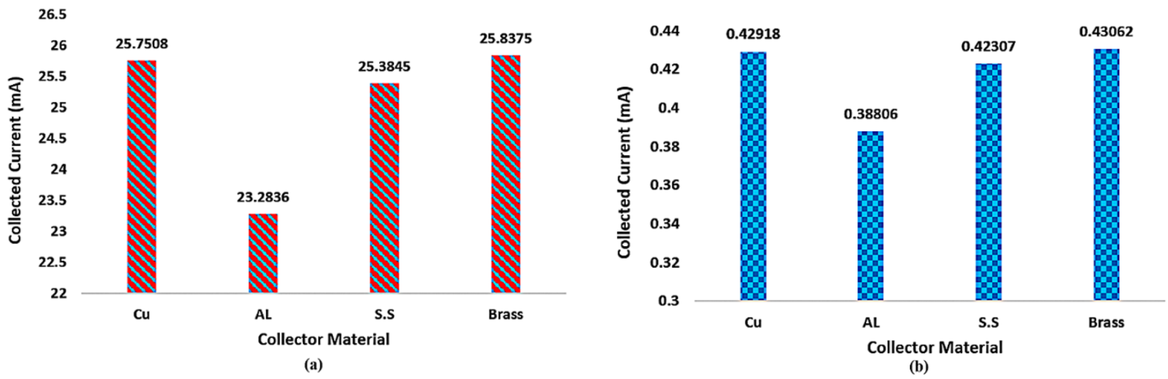

Figure 14: Collected beam current for different collector materials at (a) 30 mA and (b) 500 μA.

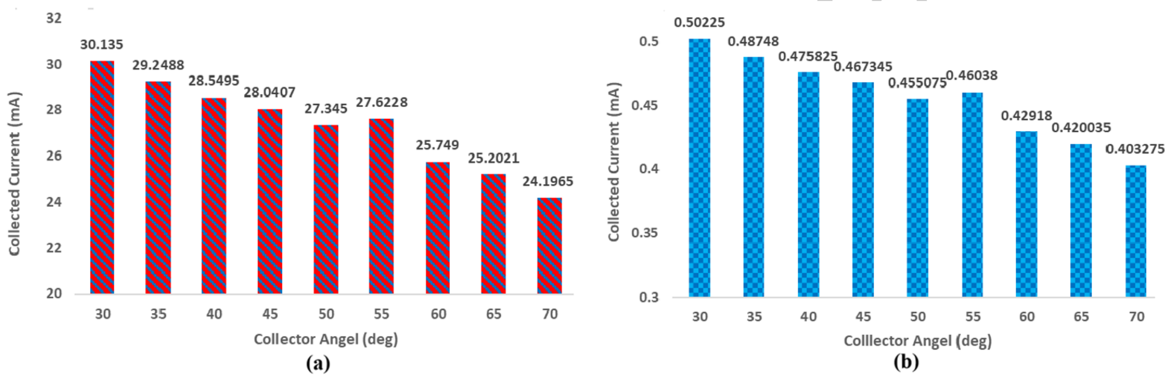

Figure 15: Collected beam current versus collector cone angle for an aluminum collector at (a) 30 mA and (b) 500 μA.

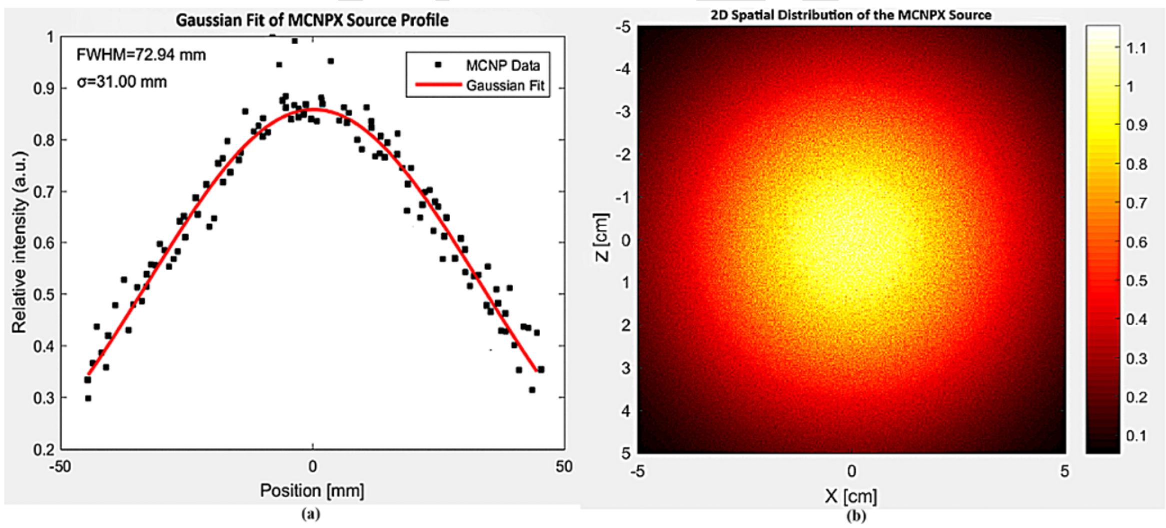

Figure 16: Proton source profiles: (a) onedimensional transverse profile with Gaussian fit, and (b) twodimensional spatial intensity distribution.

The twodimensional spatial map further demonstrates a radially symmetric Gaussianlike distribution with maximum fluence at the center and a gradual decrease toward the periphery. This confirms the absence of asymmetry or localized intensity peaks, validating the assumption of axial symmetry in the source model and ensuring welldefined initial conditions for downstream diagnostic comparisons.

4.2.1 Beam Profile Measurement Using the SEM Grid Method

The transverse beam profile was reconstructed from the current distribution measured by the SEM grid. The SEM grid consisted of 48 tungsten wires distributed across the beam cross-section with non-uniform spacing, providing adequate spatial sampling, particularly in the beam core region where intensity gradients are most significant. The resulting intensity distribution and its corresponding Gaussian fit are presented in Fig. 16.

As shown in Fig. 16, the reconstructed beam profile obtained using the SEM grid method exhibits a nearly symmetric, unimodal distribution with a well-defined maximum at the beam center and a gradual decrease toward larger transverse positions. The measured intensity distribution follows a characteristic bell-shaped curve, indicating that the extracted proton beam from the ECR ion source exhibits a stable, well-focused transverse profile under the operating conditions investigated. To quantitatively characterize the beam profile, the reconstructed data were fitted using a Gaussian function, yielding a coefficient of determination of $R^2 = 0.9975$, indicating excellent agreement between the simulation data and the Gaussian model. The fitted full width at half maximum (FWHM) was determined to be 74.53819 ± 1.9075 mm, representing the effective transverse beam width at the measurement plane. The relatively small uncertainty associated with the fitted FWHM demonstrates the stability of the fitting procedure and the reliability of the reconstructed beam profile. Furthermore, no significant deviation from the Gaussian fit was observed, in any region of the profile, indicating a stable beam distribution without noticeable asymmetry or halo formation. These results demonstrate that the SEM grid method provides reliable and repeatable reconstruction of the transverse beam profile.

4.2.2 Beam Profile Measurement Using the Slit-Faraday cup Method

To reconstruct the transverse beam profile using the slit-Faraday cup method, the transmitted beam intensity was recorded as a function of slit position as the slit was scanned incrementally across the beam cross-section. The measurement was performed at 63 discrete positions, providing a high-resolution spatial sampling of the beam intensity distribution. The resulting profile and its corresponding Gaussian fit are presented in Fig. 17.

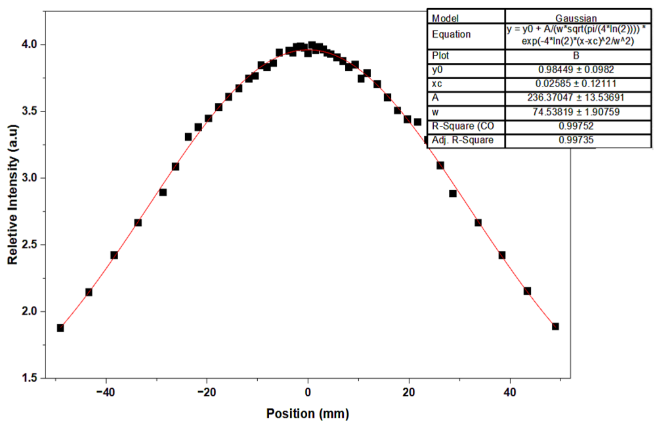

Figure 17: Reconstructed transverse beam profile obtained from the SEM grid measurements together with the corresponding Gaussian fit.

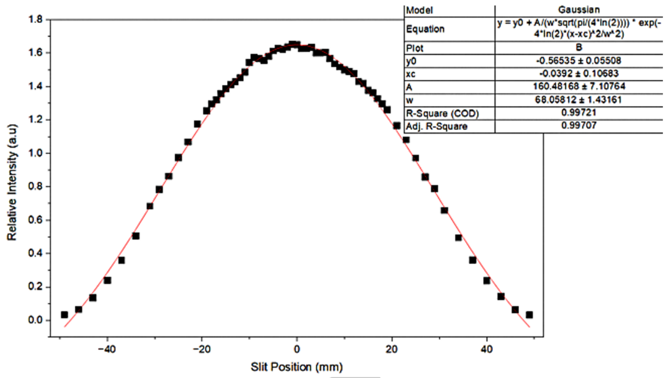

Figure 18: Reconstructed transverse beam profile obtained using the slit scanning method together with the corresponding Gaussian fit.

As shown in Fig. 17, the reconstructed beam profile obtained using the slit-scanner method exhibits a nearly symmetric, unimodal distribution with a well-defined maximum at the beam center and a gradual decrease toward larger transverse positions. The measured intensity distribution follows a characteristic Gaussian shape, consistent with the profile obtained from the SEM grid method and confirming the stability and quality of the extracted proton beam. The reconstructed data were fitted using a Gaussian function, yielding a coefficient of determination of $R^2 = 0.9972$, indicating excellent agreement between the measured profile and the Gaussian model. The fitted full width at half maximum (FWHM) was 68.0581 ± 1.431 mm, representing the effective transverse beam width at the measurement plane. The relatively small uncertainty associated with the fitted FWHM demonstrates the stability of the fitting procedure and the reliability of the reconstructed beam profile. Furthermore, no significant deviation from the Gaussian fit was observed, indicating a stable beam distribution without noticeable asymmetry or halo formation. These results demonstrate that the slit-scanner method provides reliable and repeatable reconstruction of the transverse beam profile.

4.2.3 Comparison of Beam Profile Reconstruction Methods

The beam profiles reconstructed using the SEM grid and slit-Faraday cup techniques exhibit similar overall characteristics, confirming the consistency and reliability of both diagnostic approaches. As presented in Figs. 16 and 17, both methods produce nearly symmetric, unimodal distributions that are well described by Gaussian functions. In both cases, the maximum intensity is located near the beam center, with a gradual decrease toward the beam edges, indicating a stable, well-collimated, and properly transported proton beam from the ECR ion source. Despite these qualitative similarities, a quantitative comparison of the fitted profiles reveals a notable difference in the extracted beam parameters. The slit-Faraday cup method yields a smaller FWHM of 68.0581 ± 1.431 mm, compared with 74.53819 ± 1.9075 mm obtained from the SEM grid method. This difference of approximately 6.48

mm (about 8.5%) is not attributed to measurement error or fitting inaccuracies, as both fits exhibit high coefficients of determination ($R^2 = 0.9972$ for the slit scanner and $R^2 = 0.9975$ for the SEM grid). Rather, the observed discrepancy arises from the intrinsic spatial resolution characteristics of the two diagnostic techniques. In the slit-Faraday cup method, the beam profile is reconstructed by mechanically scanning a narrow slit (0.5 mm aperture) across the beam cross-section at 63 discrete positions. This approach provides highly localized sampling of the beam intensity distribution, enabling precise determination of the beam boundaries and fine details of the profile shape. The high spatial resolution of the slit scanner allows for accurate identification of the beam edges, resulting in a more precise FWHM measurement. In contrast, the SEM grid method employs an array of 48 tungsten distributed across the measurement plane. The discrete wire structure introduces a certain degree of spatial averaging, leading to a slightly broader reconstructed profile. Nevertheless, the high coefficients of determination and the relatively small FWHM uncertainties obtained for both techniques demonstrate that the observed difference originates from the measurement principles of the two diagnostic methods rather than from reduced measurement accuracy or fitting reliability. Therefore, both techniques provide reliable beam profile characterization, while the slit-scanner offers higher spatial resolution for detailed transverse beam analysis.

4.2.4 Validation of the Simulated Beam Profile

To assess the reliability of the developed simulation framework, a dedicated validation study was conducted by comparing the simulation results with the experimentally measured beam profile reported by M. Yarmohammadi Satri et al. (Yarmohammadi Satri et al., 2014), as presented in Fig. 19. According to this figure, the Gaussian parameters of the reference profile are $\sigma = 1.28364$ mm and FWHM = 3.02274 mm, whereas the simulated Gaussian profile yields $\sigma = 1.2127$ mm and FWHM = 2.8559 mm. The relative error calculated for both σ and FWHM is 5.52%, indicating that the difference between the simulated and reference profiles remains within an acceptable range. This level of discrepancy can be attributed to natural differences between real experimental conditions and numerical modeling. In practical systems, the beam profile is influenced by various physical and operational factors that are idealized in numerical simulations. In contrast, the simulated profile is generated using a Gaussian distribution with fixed parameters representing the average beam behavior. Furthermore, geometric approximations and boundarycondition simplifications in the numerical model may introduce minor deviations between the simulated and experimental results.

Considering these factors, the observed difference is entirely reasonable and demonstrates that the simulated beam profile exhibits a reliable agreement with the reference data in terms of shape, peak width, and statistical parameters. Therefore, the numerical model employed in this study provides sufficient accuracy for subsequent analyses.

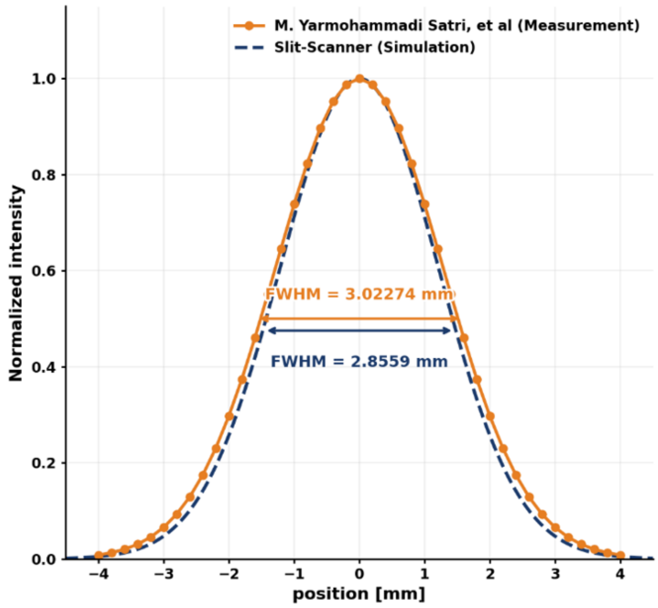

Figure 19: Validation of the slit-scanner (dashed line) simulation by comparison with the experimentally measured beam profile (dotted line) reported by M. Yarmohammadi Satri et al. (Yarmohammadi Satri et al., 2014).

5 Conclusions

In this work, a comprehensive ion beam diagnostic system consisting of a Faraday cup, a slit-scanner, and a secondary electron monitor (SEM) grid was designed, optimized and evaluated using MCNP simulations and COMSOL Multiphysics thermal analyses. The study addressed both beam current measurement and transverse beam profile characterization within a unified diagnostic framework, specifically tailored for low-energy proton beams extracted from an ECR ion source. The influence of collector material and cone angle on the Faraday cup response was systematically investigated through Monte Carlo particle transport simulations. Although the collected current exhibited only minor variations across the examined geometrical and material configurations, the results valuable insights into the interplay between collector geometry, particle confinement, and charge collection efficiency. Thermal simulations further revealed that the highest temperature concentration occurs in the conical collector region, emphasizing the necessity of an appropriate cooling strategy for reliable long-term operation. A five-turn helical water-cooling channel was designed and evaluated, demonstrating effective heat removal from the critical conical section.

Based on the combined results of the MCNP particle transport simulations, COMSOL thermal analyses, and practical engineering considerations, a 60° conical collector was selected as the optimum geometry. Although smaller cone angles exhibited slightly improved particle confinement, they also introduced significantly greater machining complexity, reduced tool accessibility, and higher fabrication costs. The 60° configuration thus provides an appropriate compromise between beam collection efficiency, thermal performance, and practical manufacturability. Among the investigated materials, aluminum was selected as the optimum collector material because it offers a balanced combination of satisfactory thermal behavior, low weight, ease of machining, and reduced fabrication cost, while maintaining reliable beam current collection. Although copper possesses superior electrical and thermal conductivity, its higher cost and greater machining difficulty make aluminum a more practical choice for the proposed design.

Beam profile reconstruction was performed using both the SEM grid and the slit-Faraday cup, and the results were compared with the intrinsic source profile obtained from MCNP. The source exhibited an FWHM of 72.94 mm, serving as the reference for evaluating the diagnostic accuracy. The SEM grid yielded an FWHM of 74.53 ± 1.90 mm, corresponding to a relative deviation of only 2.18% from the source profile, indicating that the wirebased sampling preserves the overall beam width with high fidelity. In contrast, the slitFaraday cup produced an FWHM of 68.06 ± 1.43 mm, which is 6.69% narrower than the source profile. This slight underestimation is consistent with the higher spatial resolution of the slit scanner (0.5 mm aperture and 63 sampling positions), whose localized sampling tends to emphasize the central intensity region compared with the spatial averaging inherent in the SEM grid (48 wires with 50 μm diameter).

Despite these differences, both diagnostics demonstrated excellent Gaussian conformity, with coefficients of determination of $R^2 = 0.9975$ (SEM grid) and $R^2 = 0.9972$ (slit-Faraday cup), confirming the stability, symmetry, and wellcollimated nature of the beam. The combined diagnostic system-integrating the optimized Faraday cup, SEM grid, and slit scanner-provides a robust, costeffective, and complementary solution for lowenergy ion beam characterization. The methodology, supported by particle transport simulations, thermal analysis, and engineering optimization, establishes a reliable framework that can be extended to higher energies and different ion species. Furthermore, the reliability of the developed simulation framework was assessed by comparing the simulated beam profile with the experimentally measured profile reported by M. Yarmohammadi Satri et al. (Yarmohammadi Satri et al., 2014), and the simulation. Future work will focus on experimental validation, realtime data acquisition, and expansion of the diagnostic capabilities.

Conflict of Interest

The authors declare no potential conflict of interest regarding the publication of this work.

Funding

The authors declare that no funds, grants, or other financial support were received during the preparation of this manuscript.

References

Ashcroft, N. W. and Mermin, N. D. (1976). Solid state physics.

Barale, J. J., Crebbin, K. C., Lax, J. W., et al. (1979). Secondary emission monitors at the Bevatron-Bevalac. *IEEE Transactions on Nuclear Science*, 26(3):3412–3414.

Baxter, A., Dhar, A., Gabriel, A., et al. (2025). SEM Grid Testing at NLCTA in BeamNetUS Program. Technical report, SLAC National Accelerator Laboratory; Harvey Mudd College.

Brown, I. G. (2004). *The physics and technology of ion sources*. John Wiley & Sons.

Ehwald, J., Togno, M., Lomax, A. J., et al. (2023). Detailed Monte-Carlo characterization of a Faraday cup for proton therapy. *Medical Physics*, 50(9):5828–5841.

Geller, R. (2018). *Electron cyclotron resonance ion sources and ECR plasmas*. Routledge.

Harasimowicz, J. and Welsch, C. (2010). Faraday cup for low-energy, low-intensity beam measurements at the USR. *Proc. BIW, Santa Fe, NM, USA*, pages 1–13.

Humphries, S. (2013). *Principles of charged particle acceleration*. Courier Corporation.

Minty, M. G. and Zimmermann, F. (2003). *Measurement and control of charged particle beams*. Springer Nature.

Rawat, B. S., Kumar, N., Ghosal, D., et al. (2025). Faraday cups: Principles, designs, and applications across scientific disciplines-A review. *Instruments*, 9(3):20.

Reiser, M. (2008). *Theory and design of charged particle beams*. John Wiley & Sons.

Sortais, P. (2000). Status and development of ECR ion sources. In *Proc of the EPAC*, volume 2000, page 7th.

Sun, L. (2017). Emittance Measurement of the SECRAL-II Beam Using the Slit-Faraday Cup Method, Proceedings of ECRIS2016. Technical report.

Valizadeh, R., Malyshev, O. B., Wang, S., et al. (2014). Low secondary electron yield engineered surface for electron cloud mitigation. *Applied Physics Letters*, 105(23).

Yarmohammadi Satri, M., Zocca, F., Roncarolo, F., et al. (2014). Transverse Beam Profile Measurements in the Linac4 Medium Energy Beam Transport. Technical report.

You, H., Jang, S., and Choo, W. (2015a). Beam Profile Measurements with a Slit-Faraday Cup and a Wire Scanner for a Newly Developed 18 GHz Superconducting ECR Ion Source and its LEBT. In *4th International Beam Instrumentation Conference (IBIC2015), Melbourne, Australia*, pages 113–117.

You, H., Jang, S., and Choo, W. (2015b). Beam Profile Measurements with a Slit-Faraday Cup and a Wire Scanner for a Newly Developed 18 GHz Superconducting ECR Ion Source and its LEBT. In *4th International Beam Instrumentation Conference (IBIC2015), Melbourne, Australia*, pages 113–117.

To cite this article:

T. Rahmanabadi, H. Jafari, M. Yarmohammadi Satri, Sh. Sanaye Hajari. Low energy proton beam characterization via a Slit-Scanner. *Radiation Physics and Engineering*, In Press.

DOI:

To link to this article: